METHOD COMPARISON FOR BONE DENSITY IN MULTIPLE MYELOMA PATIENTS

Michal Nohel[1,2], Martin Mezl[1], Vlastimil Valek[3], Marek Dostal[3,4], Jiri Chmelik[1]

[1]Department of Biomedical Engineering, Faculty of Electrical Engineering and Communication, Brno University of Technology, Brno, Czech Republic

[2]Department of Deputy Director for Science, Research and Education, University Hospital Ostrava, Ostrava, Czech Republic

[3]Department of Radiology and Nuclear Medicine, University Hospital Brno and Masaryk University, Brno, Czech Republic

[4]Department of Biophysics, Masaryk University, Brno, Czech Republic

Abstract

Bone mineral density (BMD) is an important indicator of bone health, particularly in patients with conditions such as multiple myeloma. This study aims to compare three methodologies for quantifying BMD in vertebral regions affected by lytic lesions: two using data from conventional CT with different corrections for tissue composition, and one using data acquired on a dual-energy CT system. Method 1 is based on conventional CT with corrections using reference values for muscle and fat, Method 2 uses conventional CT with corrections based on the measured CT values of paraspinal muscle, and Method 3 is based on dual-energy CT. The Wilcoxon signed-rank test was used for statistical comparison, as the dataset did not follow a normal distribution. The results indicated significant differences between Methods 1 and 2 for BMD in regions of interest (ROIs) within lytic lesions, while no significant differences were found for other comparisons in this group. For vertebrae affected by multiple myeloma, significant differences were found between Methods 1 and 2, and Methods 2 and 3, but not between Methods 1 and 3. In healthy vertebrae, a significant difference was found only between Methods 2 and 3. When all ROIs were combined, significant differences were found between Methods 1 and 2, and Methods 2 and 3, with no difference between Methods 1 and 3. Future research will focus on objectively assessing the accuracy of these methods by comparing their results with a calibration phantom.

Keywords

spine, bone mineral density, BMD, Multiple myeloma, spectral CT

Introduction

Bone mineral density (BMD) is pivotal for evaluating bone strength and resilience, serving as a crucial indicator of bone health and offering vital insights into the risk of osteoporosis and fractures due to bone weakening. Various diagnostic techniques, such as dual-energy X-ray absorptiometry (DXA) and Quantitative Computed Tomography (QCT), measure BMD. DXA, affordable and low in radiation, can be biased due to including soft tissue. It offers a 2D view, combining superficial cortical and internal trabecular bone. Multi-energy X-ray computed tomography provides detailed 3D mineral density distribution in trabecular bone. While QCT estimates the BMD of cortical and trabecular bone, it often lacks in assessing individual elemental components, crucial for accurate BMD calculation [1]. Multiple myeloma (MM) is a hematologic disease characterized by the abnormal growth of plasma cells in the bone marrow. This disorder commonly manifests with skeletal complications, where the presence of osteolytic bone lesions becomes a significant diagnostic criterion for tracking disease progression [2].

Identification of osteolytic lesions, a frequent presentation of the condition, is essential for promptly initiating therapy. In modern diagnostics, the incorporation of low-dose computed tomography (CT), alongside magnetic resonance imaging (MRI) and hybrid imaging modalities (particularly PET/CT), has become indispensable [3].

Dual-energy CT (DECT) is emerging as a significant player in medical imaging. This technique utilizes two distinct X-ray energy spectra for imaging purposes, facilitating energy decomposition and improving material differentiation. Unlike conventional CT (cCT) scans, DECT allows for the discrimination of photons with varying energy levels.

Spectral CT (sCT) can similarly leverage multi-energy decomposition. Manufacturers employ various technical setups, such as dual X-ray energies (the X-ray tube(s) actually emit two distinct energies) or dual-layer detectors (each with sensitivity to different X-ray energy levels). This functionality empowers the use of post-processing software to generate multiple parametric maps, including virtual monoenergetic images (VMI) [4, 5].

This paper aims to compare three different algorithms for calculating BMD using data from both healthy patients and patients with multiple myeloma. By analyzing a database of 10 patients, five with confirmed multiple myeloma and five without spinal pathology, the study seeks to evaluate the performance and accuracy of these algorithms in different clinical contexts.

Materials and Data

This study utilized an anonymized database comprising ten patients, including five oncological cases with multiple myeloma with lytic lesions in the spine (mean age 73 years, range 67–82 years, 3 female) and five patients with spine images showing a pathology-free condition (mean age 21 years, range 20–21 years, 3 female). The diagnosis of multiple myeloma was confirmed based on elevated levels of monoclonal immunoglobulin in the blood and an increased count of plasma cells in the bone marrow, in accordance with relevant guidelines. Diagnoses were reviewed by board-certified radiologists, including one with a special interest in myeloma imaging.

Data acquisition received approval from the Ethics Committee of University Hospital Brno under the application registration number NU23J-08-00027, and all patients provided informed consent. The data were acquired using Philips Healthcare IQon spectral CT (Philips Healthcare, Netherlands), in collaboration with the University Hospital Brno, Department of Radiology and Nuclear Medicine.

The scanning parameters for acquisition comprised a peak tube voltage of 100 kV, peak tube current of 10 mA, matrix size of 512×512, and slice thickness of 0.9 mm, utilizing a sharp reconstruction kernel and hybrid iterative reconstruction technique (iDose4; Philips Healthcare, Netherlands). Scans encompassed from the head to the knees, with the upper limbs positioned across the abdomen. Subsequently, the scans underwent assessment using a specialized workstation (Intellispace Portal version 12.1; Philips Healthcare, Netherlands). Diagnosis of multiple myeloma was confirmed based on elevated levels of monoclonal immunoglobulin in the blood and an increased count of plasma cells in the bone marrow, in accordance with relevant guidelines [6].

Raw spectral CT data in Spectral Base Imaging (SBI) format, a Philips-specific format, were accessible for each patient. Spectral CT facilitated the generation of conventional CT images and diverse parametric maps, such as virtual monoenergetic images at different energy levels, calcium suppression images, and more, utilizing a specialized workstation.

For this paper conventional CT images along with virtual monoenergetic images at 40, 80, and 120 keV were reconstructed. An illustration of the data is depicted in Fig. 1.
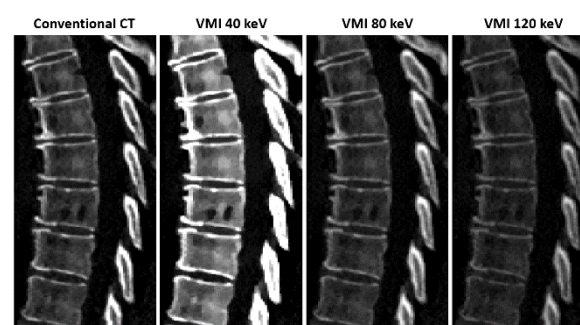

Fig. 1: Example of available data with lytic lesions (multiple myeloma disease) in different parametric images (from left conventional CT, virtual monoenergetic images (VMI) at 40 keV, VMI at 80 keV, and VMI at 120 keV), all displayed using the same window width and center.
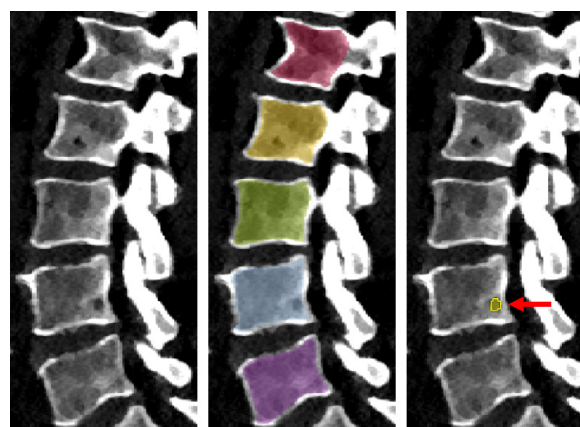

Fig. 2: Example of available lumbar spine data. On the left, a VMI image at 40 keV is displayed, in the middle a marked segmentation mask of the trabecular part of vertebrae, and on the right a segmentation mask of an analyzed lytic lesion, which is highlighted by the red arrow.

Furthermore, segmentation masks delineating the trabecular region of the L1–L5 lumbar vertebrae were accessible for each patient. These masks were

generated using the nnU-Net machine learning model, as presented at the EEICT 2024 conference [7]. Additionally, manual segmentation of lytic lesions was performed by a board-certified radiologist using the Medical Imaging Interaction Toolkit (MITK) software [8]. An illustration demonstrating the trabecular vertebrae masks and the labeled lesion is provided in Fig. 2.

Methods

In this paper, three methods for calculating bone mineral density without using a phantom were implemented and compared. The first two use conventional CT and reference tissue, where these methods assume that fat and muscle tissue, like the QCT phantom, have characteristics that are known and to some extent independent of the patient and, since they are subject to the same effects of artifacts, can be used as a reference for BMD measurements. In the third method, data from the dual-energy CT are used and the BMD value is calculated from two VMI images with different energies.

Method 1

The first method used was that published by Boden et al. [9], which is based on the assumption that the equivalent bone mineral density (ρ_{BM}) measured by QCT phantom in paraspinal muscle tissue is 27.1 mg/cm^3 and in adipose tissue −85.7 mg/cm^3 [10]. The negative value for adipose tissue arises because the mineral density is typically calibrated to different concentrations of hydroxyapatite in water, where zero equivalent bone mineral density corresponds to pure water. As adipose tissue is hypodense relative to water due to its higher carbon content, its equivalent mineral density is negative. Assuming these values are not subject to significant interpatient variability, they can be used along with their corresponding CT measurements to construct a calibration curve similar to that of a conventional external QCT phantom. By utilizing the measured CT number of the trabecular bone within this linear regression model, one can derive an estimate of the mineral density.

Method 2

The second used method is the method published by Tay et al. [11], which relies solely on the measured CT number of the paraspinal muscle to suppress the influence of different scanners and beam calibrations during each scan. This approach assumes that paraspinal muscle tissue possesses ideal characteristics that remain relatively consistent across patients, with variability mainly attributed to variations in acquisition parameters. After data correction, *CT numbers* (HU in

the equation) are converted to BMD values using the following relationship:

$$\rho_{BM} = 1.112\,HU + 47. \tag{1}$$

Method 3

The third method for calculating BMD was published by Nickoloff et al. [12] and utilizes dual-energy CT, which enables the acquisition of spectra at two different energies. This approach is based on the assumption that the trabecular part of the vertebra primarily consists of five distinct materials: bone mineral, collagen matrix, water, red marrow, and adipose tissue. Their relationships can be described by the following equation:

$$CT\ number = \alpha\rho_{BM} + \eta\rho_C + \omega\rho_W + \beta\rho_F + \theta\rho_M + \delta + \varepsilon \tag{2}$$

where α (calcium hydroxyapatite), η (collagen), ω (water), β (adipose tissue), and θ (red marrow) are attenuation coefficients dependent on photon energy, $\delta = -1000$ HU, ε is the number of offset of water, and ρ_{BM}, ρ_C, ρ_W, ρ_F, and ρ_M are concentrations of bone mineral, collagen matrix, water, adipose tissue, and red marrow, respectively, in milligrams per cubic centimeters (mg/cm^3). Using mathematical adjustments, we are able to arrive at this relationship:

$$CT\ number = \mu V_{TB} + \beta t_{VF} + \gamma g(1 - V_{TB} - V_F) + \delta + \varepsilon \tag{3}$$

where V_{TB} are volumes of bone mineral and collagen, V_F is the volume of tissue with fat, t is the density of adipose tissue (920 mg/cm^3), g is the density of fat-free tissue (1020 mg/cm^3), μ, β and γ are constants dependent on photon energy, with known pre-measured tabulated values provided for reference [10]. We can solve Equation (2), which involves two unknowns, V_F and V_{TB}, by treating it as a system of two equations. This can be achieved through the utilization of X-ray radiation with two distinct energies in a dual-energy CT system:

$$CT_H = (\mu - \gamma g)V_{TB} + (\beta t - \gamma g)V_F + \gamma g + \delta + \varepsilon \tag{4}$$

and

$$CT_L = (\mu' - \gamma' g)V_{TB} + (\beta' t - \gamma' g)V_F + \gamma' g + \delta + \varepsilon' \tag{5}$$

where (4) is the equation for higher energy radiation (CT_H is the CT number for higher energies), and (5) is the equation for lower energy radiation (CT_L is the CT number for lower energies).

From the values V_{TB}, l—the density of bone mineral (3060 mg/cm^3), and constant λ, the density of bone mineral (BMD) can be calculated using

$$\rho_{BM} = (l + V_{TB})/(1 + \lambda). \tag{6}$$

96

Results

Data from conventional CT were used to calculate BMD by methods 1 and 2, and virtual monoenergetic images at 80 and 120 keV were used to calculate BMD by method 3. BMD was calculated only in the trabecular region using available trabecular tissue segmentation masks.

An example of the available data in a conventional CT bone radiology window, accompanied by the VMI at 40 keV, showcases the vertebra of a patient diagnosed with multiple myeloma, displaying a lytic lesion, as depicted in Fig. 3. Additionally, an example of a vertebra from a patient without pathological changes in the spine is presented in Fig. 4.
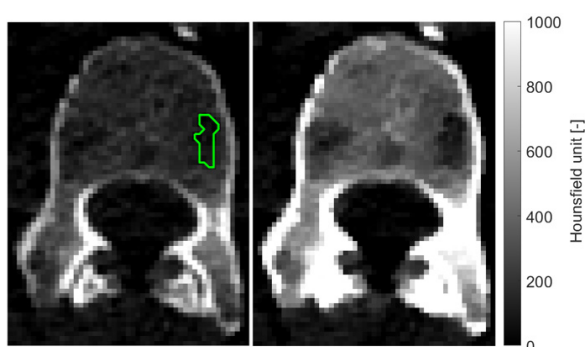
Fig. 3: Example of the first lumbar vertebra with the lytic lesion (green contour) on conventional CT (left) and VMI at 40 keV (right).
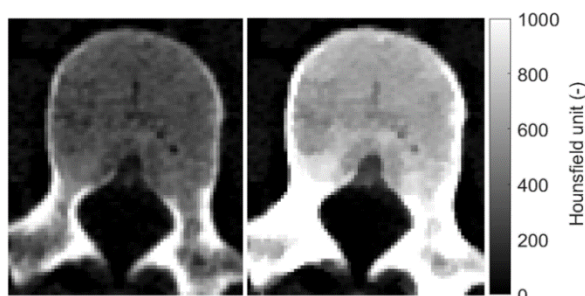

Fig. 4: Example of the first lumbar vertebra of a patient without spinal pathologies: on conventional CT (left) and VMI at 40 keV (right).

On the Fig. 5 and 6, there are illustrations of the calculated BMD maps from each method for the vertebra with the lytic lesion (Fig. 5), and for the vertebra without pathology (Fig. 6).

A total of 34 regions of interest (ROIs) were selected, of which 13 were from the trabecular part of a vertebra in a patient affected by multiple myeloma without a lytic lesion ($5 \times L1$, $5 \times L2$, $3 \times L4$), 9 ROIs were lesions identified by a radiologist ($4 \times L1$, $1 \times L3$, $3 \times L4$, $1 \times L5$), and 12 ROIs were from the trabecular region of a vertebra in a patient without spinal pathologies ($6 \times L1$, $6 \times L2$). Specifically, the ROIs from lesions consisted of entire lesions segmented by

the radiologist, while the ROIs from the vertebral regions were manually created, approximately 1 cm³, from the trabecular part of the vertebra.
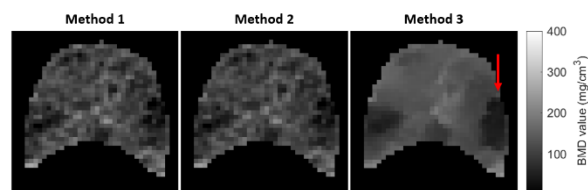

Fig. 5: Example of calculated BMD maps for first lumbar vertebra with lytic lesion, which is highlighted by the red arrow.
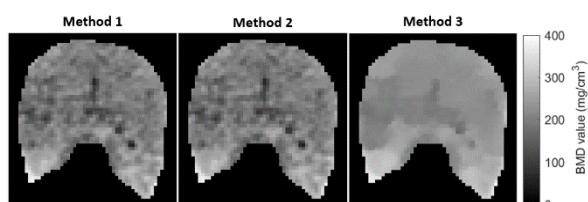

Fig. 6: Example of calculated BMD maps for first lumbar vertebra of a patient without spinal pathologies.

For each of these ROIs, the mean and standard deviation were calculated from BMD maps computed using different methods. For method comparison, box-and-whisker plots (see Fig. 7) were generated to compare the average BMD values, calculated from the created ROIs, within the identified lytic lesions and across the remaining trabecular tissue of patients with multiple myeloma, as well as with the trabecular tissue of a healthy vertebra.
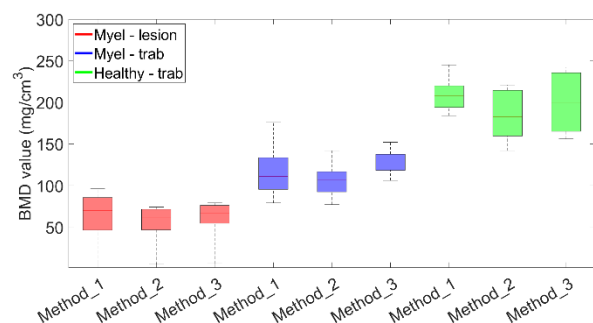

Fig. 7: The box-and-whisker plot displays the average BMD values calculated from the created ROIs. Lytic lesions are highlighted in red, ROIs from the trabecular tissue of the patient with multiple myeloma are in blue, and ROIs from healthy vertebrae are in green. Each box shows the median (central mark), 25th and 75th percentiles (bottom and top edges), and whiskers extending to the most extreme non-outlier data points.

Statistical evaluation was then conducted to determine whether the methods differed significantly. Since the data for each method comes from different types of tissue, the dataset does not follow a normal

97

distribution, and therefore, the Wilcoxon signed-rank test was used. The results of this test, including p-values for comparisons between ROIs from lytic lesions, healthy vertebrae, and vertebrae affected by multiple myeloma, as well as for all ROIs combined, are presented in Table 1.

The null hypothesis for each pair of methods (e.g., method 1 vs. method 2, method 2 vs. method 3) is that there is no significant difference between the mean values of the BMD calculated by these methods. More specifically, it assumes that the differences in BMD values between the paired methods are symmetrically distributed around zero. The Wilcoxon signed-rank test assesses whether the distribution of these differences deviates significantly from zero, indicating a significant difference between the methods.

The results, presented in Table 1, indicate that at a significance level of 0.05, methods 1 and 2 differ significantly for ROIs from lytic lesions, while no significant differences were found between other method comparisons in this group. For ROIs from vertebrae affected by multiple myeloma, statistically significant differences were observed between methods 1 and 2, and methods 2 and 3, whereas no significant difference was detected between methods 1 and 3. In the case of healthy vertebrae, a significant difference was found only between methods 2 and 3.

Furthermore, when all ROIs were combined, regardless of tissue type, the Wilcoxon signed-rank test revealed significant differences between methods 1 and 2, as well as between methods 2 and 3, but the null hypothesis was not rejected for the comparison between methods 1 and 3.

Table 1: p-values of the Wilcoxon signed-rank test for individual ROIs from lytic lesions, healthy vertebrae, and vertebrae affected by multiple myeloma, as well as for all ROIs combined, with a significance threshold set at 0.05.

Methods	M1/M2	M1/M3	M2/M3
Lesions	**0.0234**	0.5508	0.1367
ROI in MM	**<0.001**	0.2573	**<0.001**
ROI in H	0.1714	0.3110	**<0.001**
All ROIs	**<0.001**	0.8302	**<0.001**

M1—Method 1, M2—Method 2, M3—Method 3, MM—Multiple Myeloma, H—Healthy

Discussion

In recent years, Dual-Energy CT (DECT) and Spectral CT have gained traction across various medical applications due to their ability to utilize different energy spectra. This capability allows for the software-based generation of diverse parametric images, such as virtual monoenergetic images (VMI) and virtual non-contrast (VNC) images. Additionally, material decomposition techniques can be employed to emphasize or remove specific materials from the images. These advancements significantly enhance diagnostic accuracy by facilitating improved tissue characterization and the differentiation of various pathologies [13–16].

Research into the calculation of bone mineral density (BMD) using dual-energy computed tomography (DECT) has been conducted by various authors [17, 18]. These studies explore the efficacy of DECT in providing accurate and reliable assessments of BMD, which is crucial for diagnosing osteoporosis.

Our study focused on comparing three different algorithms for calculating bone mineral density (BMD), two of which utilized conventional computed tomography (CT), while one employed dual-energy CT. The algorithms were evaluated based on regions of interest (ROIs) from lytic lesions, the trabecular regions of vertebrae from patients with multiple myeloma, and the trabecular regions of healthy vertebrae.

The results indicate that methods 1 and 2 differed significantly in all cases except for the values obtained from healthy patients. Furthermore, methods 2 and 3 exhibited statistically significant differences in all instances, with the exception of ROIs from lesions. Notably, methods 1 and 3 demonstrated no significant differences according to statistical testing.

These findings suggest that while both conventional and dual-energy CT approaches can provide valuable insights into BMD assessment, the choice of algorithm may impact the results, particularly in the context of pathological conditions like multiple myeloma. Further investigations are warranted to enhance the reliability and applicability of these methods in clinical practice.

A method capable of more accurately assessing BMD could help detect earlier stages of skeletal disease, such as osteoporosis. This information would allow us to start treatment sooner and potentially improve the patient's prognosis.

One of the most common manifestations of multiple myeloma is osteolytic lesions. However, there is a wide spectrum of potential skeletal findings, including lesions in various stages of healing or extramedullary lesions. All patients in our cohort underwent a CT scan as part of the staging of newly diagnosed disease, with only a few days of targeted therapy. According to guidelines, a hypodense lesion without a sclerotic rim and <5 mm in size was defined as a myeloma bone lesion.

A key limitation of this study is the absence of phantom measurements, which are essential for validating the accuracy and precision of the BMD estimation methods. Currently, we do not have a suitable phantom available for such validation, but this will be a priority in future research. Phantoms provide a reliable baseline for comparison and allow

for a more objective assessment of each method's performance. Additionally, the lack of a universally accepted gold standard for BMD measurement complicates the evaluation of accuracy across different techniques. Without a clear reference, it is challenging to definitively establish which method is the most accurate. Future work will focus on addressing these limitations by incorporating phantom measurements and exploring appropriate benchmarks for comparison.

Another potential limitation is the bias in the dataset. The current data primarily consists of two groups: younger, healthy individuals without pathology, and older, diseased individuals with multiple myeloma and pathological skeletal changes. This raises the question of how the methods would perform in comparisons involving older individuals without skeletal pathology or younger individuals with skeletal pathology. A more balanced dataset that includes both age groups, with and without pathology, would allow for a more comprehensive evaluation of the methods. Future research should address this bias by including a broader range of patient demographics and clinical conditions.

Conclusion

In conclusion, our study utilized three approaches for calculating bone mineral density (BMD); however, it remains unclear which method is the most accurate. This uncertainty highlights the need for further research to determine the optimal algorithm for BMD assessment in various clinical contexts.

Our findings revealed statistically significant differences between some of the approaches, particularly between methods 1 and 2, and methods 2 and 3, indicating that algorithm selection may impact the assessment outcomes. However, additional investigations are required to clarify the relative accuracy and reliability of each method.

To address these questions in future studies, the verification of the algorithms will be conducted using a phantom model. By employing this approach, we aim to enhance our understanding of BMD assessment and its implications for clinical practice, particularly in populations at risk for osteoporosis and related bone health issues.

Acknowledgement

References

[1] Brett AD, Brown JK. Quantitative computed tomography and opportunistic bone density screening by dual use of computed tomography scans. Journal Of Orthopaedic Translation. 2015 Sep;3(4):178–84. DOI: 10.1016/j.jot.2015.08.006

[2] Silbermann R, Roodman GD. Myeloma bone disease: Pathophysiology and management. Journal Of Bone Oncology. 2013 Apr;2(2):59–69. DOI: 10.1016/j.jbo.2013.04.001

[3] Hillengass J, Usmani S, Rajkumar SV, Durie BG, Mateos M-V, Lonial S, et al. International myeloma working group consensus recommendations on imaging in monoclonal plasma cell disorders. The Lancet Oncology. 2019 Jul;20(6):e302–12. DOI: 10.1016/S1470-2045(19)30309-2

[4] Forghani R, De Man B, Gupta R. Dual-Energy Computed Tomography: Physical Principles, Approaches to Scanning, Usage, and Implementation: Part 1. Neuroimaging Clinics Of North America. 2017 Aug;27(3):371–84. DOI: 10.1016/j.nic.2017.03.002

[5] Rassouli N, Etesami M, Dhanantwari A, Rajiah P. Detector-based spectral CT with a novel dual-layer technology: principles and applications. Insights Into Imaging. 2017 Dec;8(6):589–98. DOI: 10.1007/s13244-017-0571-4

[6] Diagnostika a léčba mnohočetného myelomu 2023. Transfuze A Hematologie Dnes. 2023;29:1–144. [cited 2024 October 30]. Available from: myeloma.cz/res/file/guidelines/2023-transfuze-hematologie-dnes.pdf

[7] Nohel M, Chmelík J. Calculation of Bone Mineral Density from Dual-energy CT and its Application on Patient with Multiple Myeloma. Proceedings II of the 30th Conference STUDENT EEICT 2024: Selected papers, Brno: Brno University of Technology, Faculty of Electrical Engineering and Communication. 2024, 129–33. DOI: 10.13164/eeict.2024.129

[8] Wolf I, Vetter M, Wegner I, Nolden M, Bottger T, Hastenteufel M et al. The medical imaging interaction toolkit (MITK): a toolkit facilitating the creation of interactive software by extending VTK and ITK. Proc. SPIE 5367, Medical Imaging 2004: Visualization, Image-Guided Procedures, and Display. 2004 May. DOI: 10.1117/12.535112

[9] Boden SD, Goodenough DJ, Stockham CD, Jacobs E, Dina T, Allman RM. Precise measurement of vertebral bone density using computed tomography without the use of an external reference phantom. Journal Of Digital Imaging. 1989 Feb;2(1):31–8. DOI: 10.1007/BF03168013

[10] Kodým O. Analysis of 3D CT image data aimed at segmentation of bone elements and other specific tissue types [master's thesis]. [Brno]: Brno University of Technology; 2017. 74p.

[11] Tay WL, Chui CK, Ong SH, Ng AC. Osteoporosis Screening Using Areal Bone Mineral Density Estimation from Diagnostic CT Images. Academic Radiology. 2012 Oct;19(10):1273–82. DOI: 10.1016/j.acra.2012.05.017

[12] Nickoloff EL, Feldman F, Atherton JV. Bone mineral assessment: new dual-energy CT approach. Radiology. 1988 Jul;168(1): 223–8. DOI: 10.1148/radiology.168.1.3380964

[13] Alavandar E, Arunachalam VK, Narappulan N, Mahadevan GS, Kashyap R, Mehta P, et al. Principles and Available Hardware in DECT. Journal Of Gastrointestinal and Abdominal Radiology. 2022 Feb;5(2):76–84. DOI: 10.1055/s-0042-1742772

[14] Schmidt B, Flohr T. Principles and applications of dual source CT. Physica Medica. 2020 Nov;79:36–46. DOI: 10.1016/j.ejmp.2020.10.014

[15] Flohr T, Petersilka M, Henning A, Ulzheimer S, Ferda J, Schmidt B. Photon-counting CT review. Physica Medica. 2020 Nov;79:126–36. DOI: 10.1016/j.ejmp.2020.10.030

[16] Greffier J, Villani N, Defez D, Dabli D, Si-Mohamed S. Spectral CT imaging: Technical principles of dual-energy CT and multi-energy photon-counting CT. Diagnostic and Interventional Imaging. 2023 Apr;104(4):167–77. DOI: 10.1016/j.diii.2022.11.003

[17] Hammel J, Birnbacher L, Campbell G, Coulon P, Ushakov L, Pfeiffer F, et al. Comparison of volumetric and areal bone mineral density in CT and scout scans using spectral detector technology. European Radiology Experimental. 2023 Aug;7(1):37. DOI: 10.1186/s41747-023-00356-7

[18] Choi KY, Lee SW, In Y, Kim MS, Kim YD, Lee SY, et al. Dual-Energy CT-Based Bone Mineral Density Has Practical Value for Osteoporosis Screening around the Knee. Medicina. 2022 Aug;58(8):1085. DOI: 10.3390/medicina58081085

Ing. et. Ing. Michal Nohel
Department of Biomedical Engineering
Faculty of Electrical Engineering and Communication
Brno University of Technology
Technická 2058/10, CZ-616 00 Brno

E-mail: xnohel04@vutbr.cz
Phone: +420 541 146 617